

# Molecular vibrational trapping revisited: a case study with $D_2^+$

December 3, 2024

Péter Badankó (1), Gábor J. Halász (2) and Ágnes Vibók (1,3)

(1) Department of Theoretical Physics, University of Debrecen,

H-4010 Debrecen, PO Box 5, Hungary

(2) Department of Information Technology, University of Debrecen,

H-4010 Debrecen, PO Box 12, Hungary

(3) ELI-ALPS, ELI-HU Non-Profit Ltd,

H-6720 Szeged, Dugonics ter 13, Hungary

## Abstract

This article presents a detailed study of the photodissociation probability of  $D_2^+$  for a wide range of photon energy. One dimensional numerical calculations have been performed to provide the best possible physical quantities that characterize the vibrational trapping or bond hardening effect during the photodissociation dynamics. These results undoubtedly show that the nodes of the nuclear vibrational wave packets play a decisive role in the vibrational trapping, in addition to the current understating of this phenomenon.

Keywords: photodissociation; nodes; bond hardening; molecular stability; nonadiabatic effect; diatomic molecule;

# 1 Introduction

Understanding the behavior of atoms and molecules in a strong laser field is an intensively studied area and there are numerous experimental and theoretical investigations which have uncovered and explored several new phenomena of light-matter interactions including high harmonic generation, above threshold ionization or dissociation [1–4]. The bond softening and the bond hardening effects [5–24] are similar phenomena which are often visualized during the photodissociation or photofragmentation processes of diatomic or polyatomic molecules. The mechanism of bond softening is well known; was first experimentally discovered in the dissociation spectra of the  $H_2^+$  and  $D_2^+$  ions by Bucksbaum and coworkers [11–13] and can easily understand by the illustrative Floquet’s picture [25, 26] or dressed state representation, which is often used to explain various strong field physics phenomena. The Floquet Hamiltonian for the net absorption of one photon can be represented by a  $2 \times 2$  matrix, which explicitly includes the light-matter interaction. The change of the nuclear dynamics, due to the laser field, can be visualized as arising from “light-induced” or “adiabatic” molecular potentials (LIP) [27]. The molecular potential deforms due to strong radiative coupling and results in a strongly enhanced dissociation rate. The adiabatic curves show that as the laser intensity increases, the dissociation barrier moved to lower vibrational levels, leading to a noticeable growth of the dissociation probability. Bond hardening, which is often called molecular stabilization or vibrational trapping is the opposite effect with the same origins. There still remained some unresolved issues despite numerous experimental and theoretical works that have been performed in order to gain a better qualitative understanding of the mechanism behind this phenomenon [5–15, 28–30, 42].

Recent efforts have invested the nature of the light-induced conical intersections (LICIs) [30, 31] which was first discussed for diatomics by applying Floquet representation. In a diatomic molecule, which has only one nuclear vibrational coordinate, it is not possible for two electronic states of the same symmetry to form a conical intersection (CI). However, this only is true in field-free space as conical intersections can be formed, even in diatomic molecules, if an additional degree of freedom e.g. rotation, is associated with the system exposed to strong laser fields. In this situation, the interaction of the transition dipole moment of the molecule with the external electric field leads to an effective torque toward the polarization direction of the light. By considering the rotational

coordinate in the dynamical description as a dynamical variable, the change of nuclear dynamics due to the external light can be considered as arising from a LICI. The position of these LICIs are determined by the laser frequency while the laser intensity controls the strength of the nonadiabatic coupling. Several theoretical and experimental works have demonstrated that the LICIs have strong impact on the spectroscopic and dynamical properties of molecules [32–48].

There are many topical studies investigating the dissociation process of the  $D_2^+$  molecule within the LICI framework [36–40]. These use relatively small intensities ( $1 \times 10^{11}$  to  $1 \times 10^{12}$  W/cm<sup>2</sup>) and propagating the dynamics of the  $D_2^+$  resulting in very small (practically zero) rates for the dissociation probabilities of the photofragments [38] for certain vibrational eigenstates. The dissociation yield still remains relatively small even at the highest studied intensity ( $1 \times 10^{14}$  W/cm<sup>2</sup>). Obtained results are almost independent of the origins of the initial nuclear wave packet, which can start from a vibrational eigenstate or a superposition of eigenstates, the Franck - Condon, (FC) distribution, of the  $D_2^+$ . Situation is quite the similar, the frequency of the laser pulse is varied with a fixed laser intensity [38].

Intensity variation with fixed frequency was intensively theoretically studied by Bandrauk and coworkers regarding the vibrational trapping phenomenon in the  $H_2^+$  and  $D_2^+$  ions [5–8, 27]. They highlighted that laser-induced avoided crossings provide a very important source for molecular stabilization and hence suppresses dissociation at high intensities. They also found that when the diabatic (field-free) and the adiabatic (light-induced) vibrational levels coincide, the resulting resonances can minimize the photodissociation probabilities. Increasing the field intensities, trapping of the initial state into stable adiabatic states occurs due to the decreasing non adiabatic couplings between the light-induced states at high intensities. Their work resulted in a quantitatively correct picture of the vibrational trapping phenomenon mechanism.

In this article we investigate why, in certain situations, there is virtually no dissociation rate of the photofragments arising from the dissociation process of the  $D_2^+$  molecule. This paper expands previous investigations by trying to find a more accurate and quantitative connection between physical quantities including the coincidence of the diabatic and adiabatic vibrational levels; maximum overlaps between the diabatic and adiabatic wave functions and minima of the photodissociation

probabilities. This is realized by numerical simulations performed with a wide range of photon energies (from  $\omega_1 = 24.799$  eV,  $\lambda_1 = 50$  nm to  $\omega_2 = 3.100$  eV,  $\lambda_2 = 400$  nm) in order to calculate the differences of the diabatic and adiabatic vibrational energies; the diabatic and adiabatic wave functions overlap and the dissociation yields of the molecular photofragments. The results are then carefully analyzed and discussed in the light of improving the quantitative understanding of vibrational trapping.

## 2 Theory and methods

Figure 1 shows the potential energy curves for  $D_2^+$  in dressed state representation. The electronic ground ( $V_1(R) = 1s\sigma_g$ ) and the first excited ( $V_2(R) = 2p\sigma_u$ ) eigenstates are considered as diabatic potentials and together, with the kinetic energy, form the field free Hamiltonian.

$$H_{diabatic}^{f-free} = \begin{pmatrix} -\frac{1}{2\mu} \frac{\partial^2}{\partial R^2} + V_1(R) & 0 \\ 0 & -\frac{1}{2\mu} \frac{\partial^2}{\partial R^2} + V_2(R) \end{pmatrix} \quad (1)$$

where  $R$  is the vibrational coordinate and  $\mu$  is the reduced mass. The ion is excited by a resonant laser pulse from the  $V_1(R)$  ground state to the repulsive  $V_2(R)$  state. An electronic transition occurs due to nonvanishing transition dipole moment and adiabatic or light-induced states are formed resulting in the corresponding  $2 \times 2$  field dressed Hamiltonian matrix

$$H_{dressed} = \begin{pmatrix} -\frac{1}{2\mu} \frac{\partial^2}{\partial R^2} + V_1(R) & (\epsilon_0/2)d(R) \cos \theta \\ (\epsilon_0/2)d(R) \cos \theta & -\frac{1}{2\mu} \frac{\partial^2}{\partial R^2} + V_2(R) - \hbar\omega \end{pmatrix}. \quad (2)$$

The off-diagonal elements of eq. (2) represents the radiative couplings, where  $\epsilon_0$  is the maximum laser field amplitude,  $\omega$  is the laser frequency which couples the two electronic states,  $d(R)$  is the transition dipole and  $\theta$  is the angle between the polarization direction of the light and the direction of the molecular axes. The potential energies of  $V_1(R)$  and  $V_2(R)$  and the transition dipole moment were sourced from refs. [49] and [50]. The exact, time-dependent (TD) form of eq. (2), which is used extensively in the time-dependent calculations is also given here

$$H_{TD} = \begin{pmatrix} -\frac{1}{2\mu} \frac{\partial^2}{\partial R^2} + V_1(R) & \epsilon_0 f(t) d(R) \cos \theta \cos \omega t \\ \epsilon_0 f(t) d(R) \cos \theta \cos \omega t & -\frac{1}{2\mu} \frac{\partial^2}{\partial R^2} + V_2(R) \end{pmatrix} \quad (3)$$

where  $f(t)$  is the envelop function of the laser pulse.

A convenient and approximate form for the adiabatic potential is assumed. The energy levels and the eigenfunctions of the upper adiabatic potential can easily be calculated for weak fields from a model potential (Figure 2):

$$H_{adiabatic}^{upper} = -\frac{1}{2\mu} \frac{\partial^2}{\partial R^2} + (V_2 - \hbar\omega) \cdot \Theta(R_{CR}(\lambda) - R) + V_1 \cdot \Theta(R - R_{CR}(\lambda)) \quad (4)$$

where  $\Theta$  is the Heaviside step function,  $\lambda$  is the wavelength and  $R_{CR}$  is the crossing point between the ground  $V_1(R)$  and the field dressed  $(V_2(R) - \hbar\omega)$  excited states. This model potential eq. (4) can be converted into the upper adiabatic potential at zero-field limit. It is now possible to calculate the vibrational energy levels ( $E_\nu$ ) and wave functions ( $\psi_\nu$ ) belonging to the different vibrational eigenstates of the diabatic potential eq. (1) and the eigenvalues ( $\mathcal{E}_{\nu'}$ ) and eigenfunctions ( $\varphi_{\nu'}$ ) of the upper adiabatic potential eq. (4). A more detailed analysis requires new quantities derived from different combinations of the previously determined basic quantities. These are the difference of the adiabatic and diabatic eigenvalues

$$\Delta E_{\nu,\nu'}(\lambda) = \mathcal{E}_{\nu'} - E_\nu; \quad (5)$$

the adiabatic and diabatic eigenfunctions overlap,

$$S_{\nu,\nu'}(\lambda) = \langle \varphi_{\nu'}(\lambda, R) | \psi_\nu(R) \rangle = \int_{-\infty}^{\infty} \varphi_{\nu'}^*(\lambda, R) \psi_\nu(R) dR \quad (6)$$

and the total dissociation probability:

$$P_{diss} = \int_0^{\infty} dt \langle \psi(t) | W | \psi(t) \rangle, \quad (7)$$

where the  $\Delta E_{\nu,\nu'}(\lambda)$  and  $S_{\nu,\nu'}(\lambda)$  were determined with a spacing of  $\Delta\lambda = 1.0$  in the interval of (50

nm – 400 nm),  $iW$  is the complex absorbing potential (CAP) discussed in [52] and employed at the last 5 a.u. of the grid.

The multi-configuration time-dependent Hartree (MCTDH) method [51–55] is used to solve the time-independent and time-dependent Schrödinger equations in conjunction with the eigenvalue and eigenfunction problems in the diabatic/adiabatic frameworks, eqs. (1) and (4) and the dissociation dynamics eq. (3). Fast Fourier transformation-discrete variable representation (FFT-DVR) is used to characterize the vibrational degree of freedom, with  $N_R$  basis elements for the internuclear separation distributed within the range from 0.1 a.u. to 10.05 a.u. or 80 a.u. in the eigenstates or the dissociation yield calculations, respectively. These primitive basis sets ( $\chi$ ) are used to represent the wave function

$$\psi(R, t) = \sum_{l=1}^{N_R} c_{j_R l}^{(R)}(t) \chi_l^{(R)}(R). \quad (8)$$

In the actual calculations,  $N_R = 256$  is used for the eigenstates and  $N_R = 2048$  for the dynamical calculations, respectively.

### 3 Results and discussion

Our present studies intensively probe the effect of molecular stabilization using accurate numerical calculations, performed on a wide range of energies. Detailed analysis is performed using a one dimensional (1D) nuclear dynamical simulation and the initial nuclear wave packet is assumed to be in one of the vibrational eigenstates ( $\nu = 0, 1, 2, 3, 4, 5, 6, 7, 8, 9$ ) or Franck-Condon distribution of the vibrational states of the ion. The initial orientation of the molecules is assumed to be parallel to the external field in all cases. The dissociation rates for isotropic initial distribution can be approximated with large accuracy by dividing the results by 3 as this study is limited to low intensities. The energy interval ( $\omega_1 = 24.799$  eV,  $\lambda_1 = 50$  nm to  $\omega_2 = 3.100$  eV,  $\lambda_2 = 400$  nm) is chosen to be contained all the values belonging to the positions of the near zero dissociation probability of the studied vibrational levels. A linearly polarized Gaussian laser pulse, with intensity,  $I_0 = 10^{11} \text{ W/cm}^2$  and a pulse duration in full width at half-maximum (FWHM)  $t_{pulse} = 30$  fs is used throughout the calculation.

Three physical properties, the difference of the diabatic and adiabatic eigenvalues ( $\Delta E(\lambda)$ ); the the diabatic and adiabatic eigenfunctions ( $S(\lambda)$ ) overlap and the dissociation probability ( $P_{diss}$ ) play an important role in the forthcoming analysis.

### 3.1 Dissociation probability, wave function overlap and energy difference

The dissociation probability, eq. (7) is calculated in the chosen energy interval by maintaining a fixed light intensity. Wavelengths which results in a virtually zero dissociation probability from a particular vibrational energy level are sought, like previous investigations [38]. Calculations have been performed for all chosen vibrational eigenstates,  $\nu = 0, 1, \dots, 9$ , and the previously determined energy interval ensured that for each eigenstates all the wavelengths which belong to a minimum value of the dissociation probability were assigned. For example, nine different values for the wavelength were found for the  $\nu = 9$  vibrational level .

Figure 3 shows the results for the  $\nu = 4$  vibrational level for the case when the initial nuclear wave packet starts from (i) a vibrational eigenstate or from (ii) a superposition of eigenstates, the Franck - Condon, (FC) distribution, of the  $D_2^+$ . The dissociation rate has four minima at the  $\lambda_D(4, 3) = 88.8$  nm,  $\lambda_D(4, 2) = 112$  nm,  $\lambda_D(4, 1) = 139.5$  nm and  $\lambda_D(4, 0) = 177.1$  nm wavelengths. Simulations in which the wave packets start from a vibrational eigenstate pulses with a 30 fs length centered around 0 fs are used and the total dissociation probabilities are calculated. In the second superposition situation pulses with a 30 fs length centered around 34 fs are applied and approximately one and half vibration cycle taking place during 34 fs on the diabatic lower surface  $V_1$  [37]. The yield of total dissociation probability does not provide any information about the dissociation rate resulting from a particular vibrational state because all of the vibrational eigenstates are included in the initial wave packet. Thus, attention turned to the kinetic energy (KER) release spectra and the dissociation rate at the  $E_\nu + \hbar\omega$  energy was studied. The results clearly show that there is virtually no difference between vibrational (i) and superposition (ii) situations. This indicates, that the structure of the initial wave packet does not significantly affect of the underlying physical mechanism and thus, only the initial wave packets in vibrational eigenstate form are used in further calculations.

The next task was to obtain the diabatic and adiabatic eigenfunctions overlap which was calcu-

lated using eq (6). For each diabatic vibrational level ( $\nu$ )  $\nu' = 0, 1, \dots, \nu - 1$ , adiabatic eigenstates and correspondingly  $\nu$  different overlap functions exist. Figure 4 shows these functions for the  $\nu = 4$  vibrational level. The 4 different panels belong to the four corresponding values of  $\nu'$  from 0 to  $\nu - 1$ , and obtained curves are scaled on left side of the panels.

The difference of the adiabatic and diabatic eigenvalues eq (5), is determined and  $\nu$  energy difference curves are obtained for each value of  $\nu$ . Figure 4 shows these curves which are scaled on right side of the panels. It can be expected, based on previous theoretical studies [8, 9, 27] that, for a given pair of diabatic and adiabatic eigenstates with the feature of  $\nu > \nu'$ , both the maxima of the overlap between the diabatic and adiabatic vibrational wave functions at  $\lambda = \lambda_O(\nu, \nu')$  and the matching of the diabatic and adiabatic eigenvalues at  $\lambda = \lambda_E(\nu, \nu')$  are closely related to the minimal dissociation yield or bond hardening situation, which takes place at special photon energies  $\lambda = \lambda_D(\nu, \nu')$ . These special values of the wavelength are presented in the first four columns of Table 1 for all the studied vibration levels ( $\nu = 0, 1, \dots, 9$ ). If the values of these three wavelengths ( $\lambda_D$ ,  $\lambda_O$  and  $\lambda_E$ ) for a certain pair of vibrational frequency ( $\nu, \nu'$ ) are close to each other, the values of the  $\frac{\lambda_O}{\lambda_D}$  and  $\frac{\lambda_E}{\lambda_D}$  ratios are also close to 1. However, figure 5 shows that this is not the case as the  $\frac{\lambda_O}{\lambda_D}$  and  $\frac{\lambda_E}{\lambda_D}$  wavelength rates for all case systematically deviate from 1 within a range of 5%–15%. The significantly large differences between the wavelengths suggests that the physics behind the trapping effect may not be described adequately by studying the overlap of the wave functions or energy differences and it is expected, that some other factors may play a role.

### 3.2 The role of the nodes

This section starts with a simple analysis of the adiabatic and diabatic wave functions overlap. It is obvious that the node positions of adiabatic wave function should be close to the node positions of the diabatic function in order to obtain a significantly large overlap. The adiabatic wave function fades to zero at small internuclear distances where the adiabatic potential is above to the adiabatic energy level. By applying photon energy resulting in the dissociation minimum yields similar energies of the diabatic and adiabatic states. In such a case, the disappearance of the adiabatic wave function can be expected to approximately take place where the adiabatic potential is equal to the energy



of the diabatic eigenstate. Thus, it can be assumed that for a large overlap the matching of the adiabatic potential to the diabatic energy level should be taken place around one of the nodes of the diabatic eigenfunction. The wavelength  $\lambda_{E_\nu}(\nu, \nu')$  is where the matching of the adiabatic potential to the energy of the diabatic eigenstate takes place at the  $(\nu - \nu')^{th}$  node ( $R_n(\nu, \nu')$ ) of the diabatic wave function, i.e., after which there are additional  $\nu'$  nodes (Figure 6):

$$\hbar\omega_{E_\nu} = V_2(R_n(\nu, \nu')) - E_\nu. \quad (9)$$

There is another possible way to demonstrate the importance of the nodes of the nuclear wave packet in the process of molecular stabilization. In the light-induced picture of dissociation, the nonadiabatic coupling between the two surfaces will be the largest around the crossing of the ground and the dressed excited state diabatic potentials. Therefore, a reasonable reduction in the dissociation yield can be expected if the initial diabatic wave packet has a node at, or close to this crossing. To check the validity of this approach, the wavelengths for which the crossing of the potentials takes place at one of the nodes of the diabatic wave function was determined. These values are denoted as  $\lambda_\times(\nu, \nu')$  and the corresponding photon energies can be calculated as

$$\hbar\omega_\times = V_2(R_n(\nu, \nu')) - V_1(R_n(\nu, \nu')). \quad (10)$$

Table 1 shows both of these newly introduced quantities and the positions of their dependant nodes.

The accuracy of the above constructed approach was checked by calculating the ratios with  $\lambda_D$  and the obtained  $\frac{\lambda_\times}{\lambda_D}$  and  $\frac{\lambda_{E_\nu}}{\lambda_D}$  rates are shown in Figure 5a. For lower lying vibrational states, both these two new formulas, based on the position of the nodes, provide a better forecast for the wavelength of the minimal dissociation yield than the preliminary defined  $\lambda_E$  or  $\lambda_O$  values.  $\lambda_\times$  under estimates  $\lambda_D$  approximately twice as much as  $\lambda_{E_\nu}$  over estimates it. This observations have resulted in some additional new quantities: the weighted arithmetic, geometric and harmonic means (arithmetic mean of the photon energies) of the former two node based approximations for the position of the minimal

dissociation rate:

$$\bar{\lambda}_a = (\lambda_{\times} + 2\lambda_{E_{\nu}})/3 \quad \Longleftrightarrow \quad \bar{\omega}_a = \frac{3}{1/\omega_{\times} + 2/\omega_{E_{\nu}}}, \quad (11)$$

$$\bar{\lambda}_g = \sqrt[3]{\lambda_{\times} \cdot \lambda_{E_{\nu}}^2} \quad \Longleftrightarrow \quad \bar{\omega}_g = \sqrt[3]{\omega_{\times} \cdot \omega_{E_{\nu}}^2}, \quad (12)$$

$$\bar{\lambda}_h = \frac{3}{1/\lambda_{\times} + 2/\lambda_{E_{\nu}}} \quad \Longleftrightarrow \quad \bar{\omega}_h = (\omega_{\times} + 2\omega_{E_{\nu}})/3. \quad (13)$$

The ratios of the above constructed mixed quantities to the dissociation minimum ( $\lambda_D$ ) are shown in Figure 5b. All the three formulas lead to very similar results predicting the dissociation minima with less than a half percent error, except for a few cases. The harmonic mean, defined in eq. (13), is the most balanced combination as its values remain in the narrowest interval around  $\lambda_D$ . The fact that these wavelengths, especially their special combination provide an almost perfect molecular stability, implies that the nodes of the nuclear vibrational wave packet play an essential role in the bond hardening effect.

The above numerical results support the theoretical expectations: initiating the nuclear dissociation dynamics from a given vibrational level, one can always find the appropriate photon energy that minimizes the dissociation yield. The latter holds for the total dissociation probability when the initial wave packet starts from one of the vibrational eigenstates and for the kinetic energy release spectra (KER) at a certain ( $E_{\nu} + \hbar\omega$ ) energy when the initial wave packet starts from a FC distribution of ionic vibrational eigenstates. At the heart of this work are the nodes of the nuclear vibrational wave packet which can quantitatively be associated with the bond hardening effect.

The example throughout this study was the  $D_2^+$  molecule and we believe that these results from the reported numerical calculations can be applied to general systems and that these present findings are independent from  $D_2^+$  and are valid for any other molecular systems.

## 4 Conclusions

In this paper, a series of numerical calculations, over a wide range of photon energies, have been performed and analyzed in order to provide very accurate results for the vibration trapping phenomenon. It has demonstrated that the nodes of the nuclear vibrational wave packets have an important role in

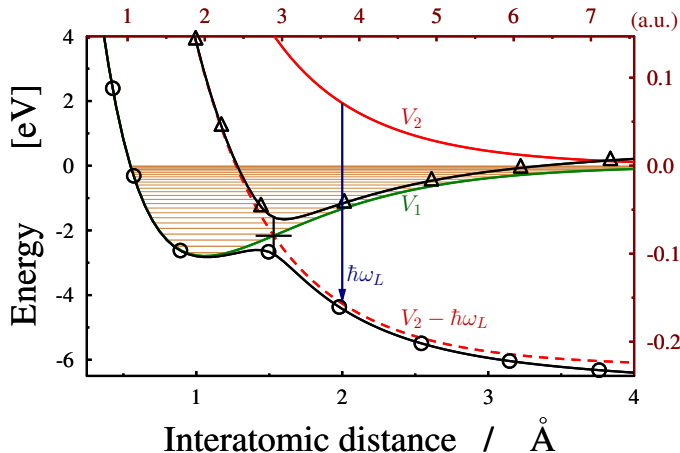


Figure 1: A cut through the potential energy surface of the  $D_2^+$  molecule as a function of inter atomic separation. Diabatic energies of the ground ( $V_1$ ) and the first excited ( $V_2$ ) states are displayed with solid green and red lines, respectively. The field dressed excited state ( $V_2 - \hbar\omega_L$ ; dashed red line) forms a light induced conical intersection (LICI) with the ground state. For the case of a laser frequency  $\omega_L = 6.199 \text{ eV}$  and field intensity of  $3 \times 10^{13} \frac{W}{cm^2}$  a cut through the adiabatic surfaces at  $\theta = 0$  (parallel to the field) is also shown by solid black lines marked with circles ( $V_{lower}$ ) and triangles ( $V_{upper}$ ). The position of the LICI is indicated with a cross.

the molecular stabilization process. We have found an accurate quantitative connection between the nodes of the nuclear vibrational wave packet and the minimum of the dissociation rate. In contrast to the literature, the importance of the nodes of the vibrational wave packet is strongly stressed because an almost perfect molecular stabilization can be obtained using our recently proposed formula eq. (13) of the node based wavelength.

However, we have yet to clearly identify the background mechanism behind the harmonic mean combination of the  $\lambda_{E_\nu}$  and  $\lambda_\times$  wavelengths, which can provide the best description of the phenomena. Our studies will continue and be extended in this direction and we expect to form a better understanding about the complex physical phenomena beyond the vibrational trapping effect. Nevertheless, we hope that these present findings will stimulate experimental works in the near future.

## Acknowledgment

B. P. acknowledges the TÁMOP-4.2.2.B-15/1/KONV-2015-0001 ‘National Excellence Program’. Á.V. acknowledges the OTKA (NN103251) project. The supercomputing service of NIIF has been used for this work. The authors thank Lorenz Cederbaum for many fruitful discussions.

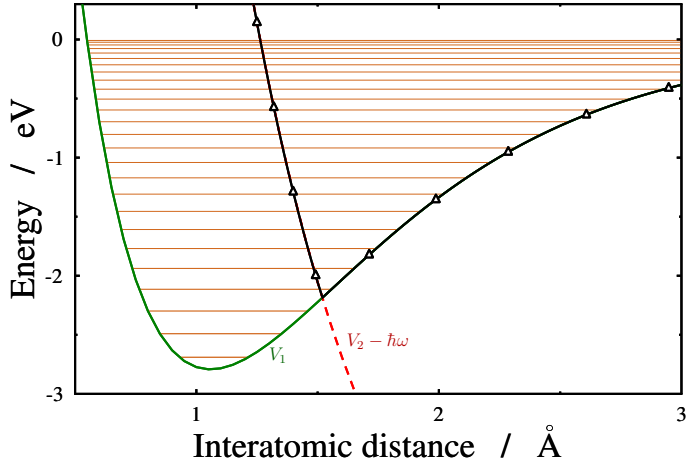


Figure 2: Diabatic and adiabatic cut of the potential energy surfaces along the inter atomic separation. Diabatic energies of the ground ( $V_1$ ; solid green) and the field dressed excited ( $V_2 - \hbar\omega_L$ ; dashed red line) states are displayed. The adiabatic upper curve –calculated by using eq. (4) for the weak field limit– is denoted by solid black line marked with triangles. The different horizontal lines provide the appropriate diabatic (in orange) vibrational energy levels.

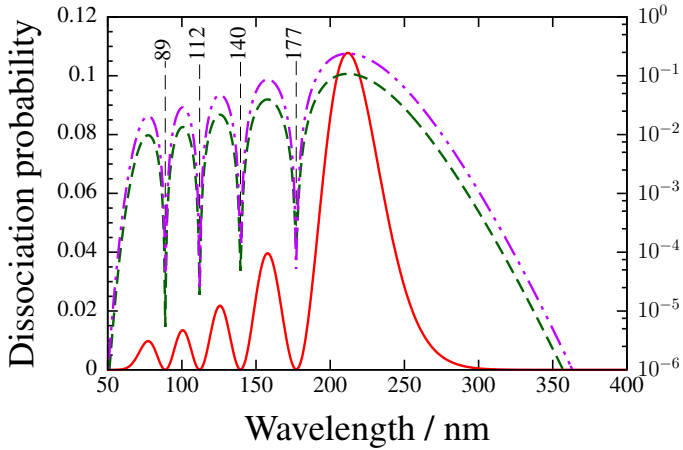


Figure 3: Total dissociation probabilities as a function of laser wavelength for  $\nu = 4$  vibrational eigenstate. The applied energy/wavelength interval and the intensity are from  $\hbar\omega_1 = 24.798 \text{ eV}$ ,  $\lambda_1 = 50 \text{ nm}$  to  $\hbar\omega_2 = 3.0998 \text{ eV}$ ,  $\lambda_2 = 400 \text{ nm}$  and  $I = 1 \times 10^{11} \frac{\text{W}}{\text{cm}^2}$ , respectively. The total dissociation probability from the  $\nu = 4$  vibrational eigenstate is displayed by the solid (linear scale on the left side) and dashed (logarithmic scale on the right side) curves. The dashed-dotted curve displays (logarithmic scale on the right side) the differential dissociation rate with kinetic energy of fragments being  $E_\nu + \hbar\omega$  when the simulation was started from Franck-Condon distribution.

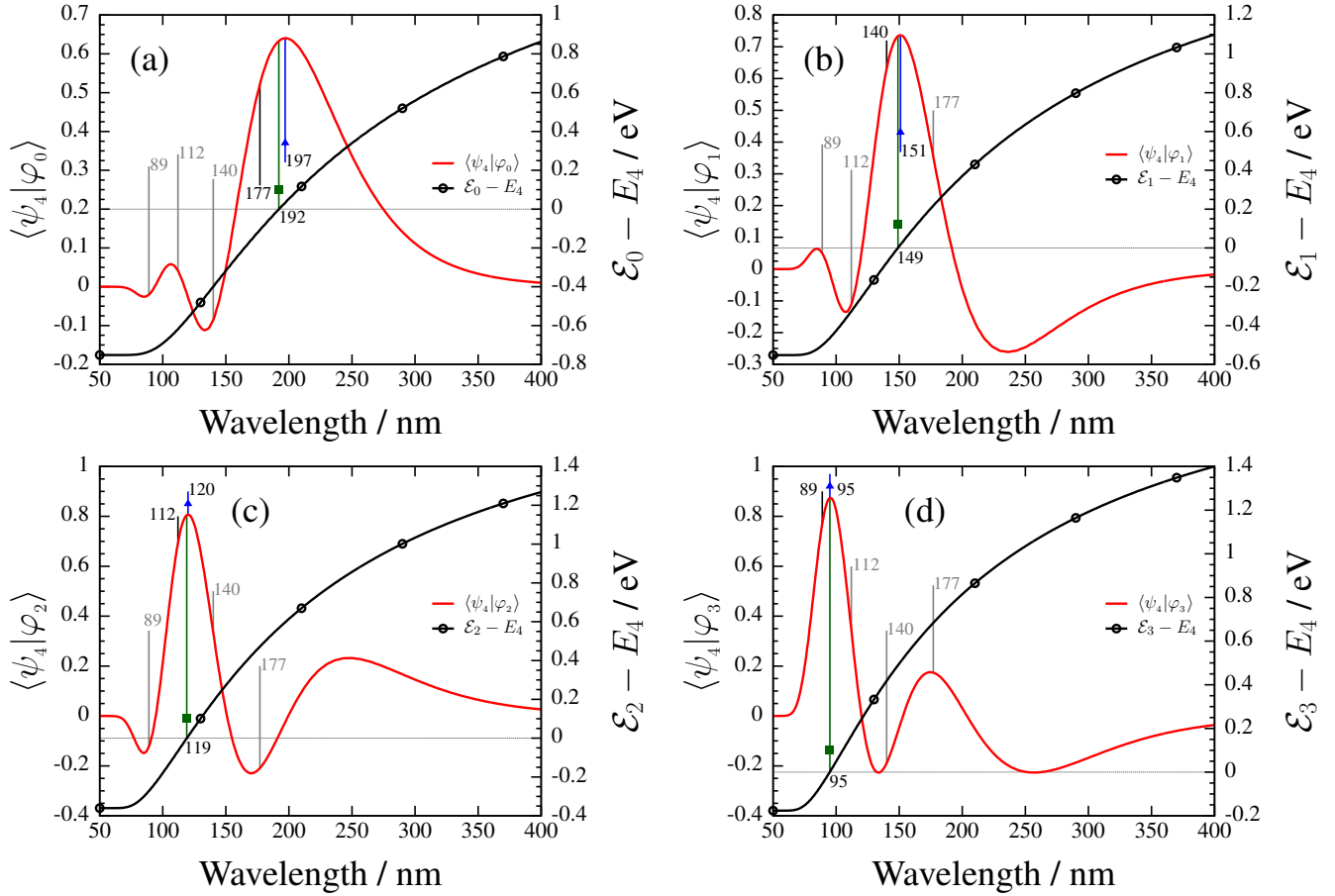


Figure 4: Overlap  $S_{\nu, \nu'}(\lambda)$  between the diabatic ( $\psi_\nu$ ;  $\nu = 4$ ) and adiabatic ( $\varphi_{\nu'}$ ) eigenfunctions and the difference of the diabatic and adiabatic eigenvalues ( $\Delta E_{\nu, \nu'}(\lambda) = \mathcal{E}_{\nu'} - E_\nu$ ;  $\nu = 4$ ) as a function of wavelength. The value of  $S_{\nu, \nu'}(\lambda)$  (solid curve) is given by the scale on the left side, while the value of  $\Delta E_{\nu, \nu'}(\lambda)$  (dotted curve) is given by the scale on the right side. Bars denote the wavelengths for which the total dissociation probability is minimal. Bars with triangle and bars with square present the  $\lambda_O(\nu, \nu')$  and  $\lambda_E(\nu, \nu')$  wavelengths corresponding to the maximum value of  $S_{\nu, \nu'}(\lambda)$  and the zero value of  $\Delta E_{\nu, \nu'}(\lambda)$ , respectively. In panel A ( $\nu' = 0$ ), in panel B ( $\nu' = 1$ ), in panel C ( $\nu' = 2$ ) and in panel D: ( $\nu' = 3$ ).

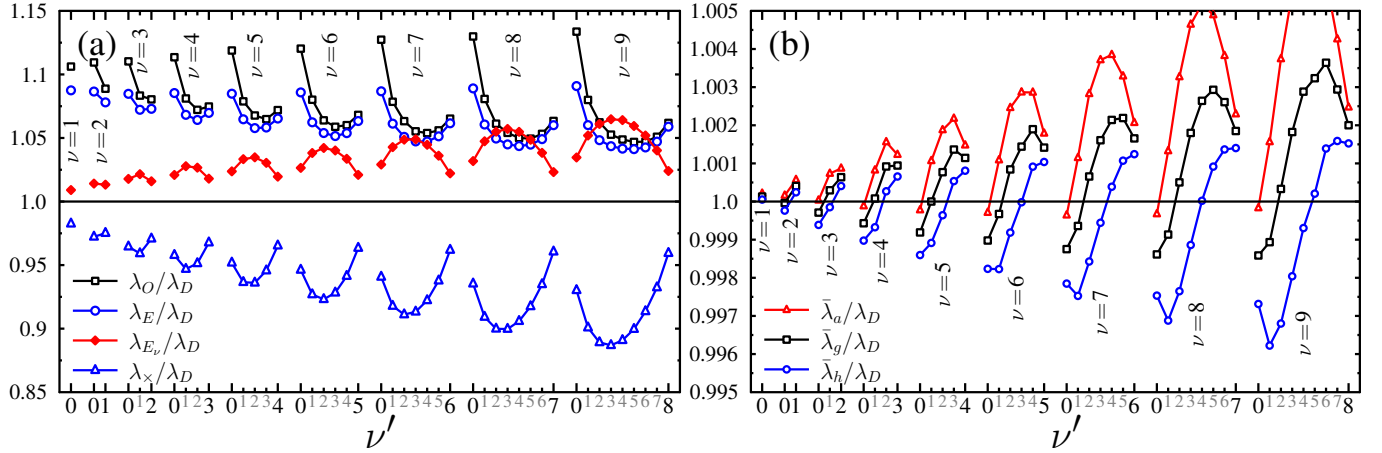


Figure 5: Ratios of the different wavelengths respect to the minimum value of the dissociation probability  $\lambda_D$ . Panel A:  $\lambda_O$  is the wavelength belongs to the maximum value of the wave functions's overlap,  $\lambda_E$  is the wavelength where the adiabatic and diabatic eigenvalues are the same,  $\lambda_{E\nu}$  is the wavelength according to eq. (9) and  $\lambda_\times$  is the wavelength according to eq. (10); Panel B:  $\bar{\lambda}_a$ ,  $\bar{\lambda}_g$  and  $\bar{\lambda}_h$  are the weighted arithmetic, geometric and harmonic means of  $\lambda_{E\nu}$  and  $\lambda_\times$  as defined in eqs. (11–13).

$\nu, \nu'$	$\lambda_D (nm)$	$\lambda_O (nm)$	$\lambda_E (nm)$	$\lambda_{E\nu} (nm)$	$\lambda_\times (nm)$	$R_n (au)$	$\nu, \nu'$	$\lambda_D (nm)$	$\lambda_O (nm)$	$\lambda_E (nm)$	$\lambda_{E\nu} (nm)$	$\lambda_\times (nm)$	$R_n (au)$
1,0	111.21	123.02	120.94	112.21	109.27	2.05	7,0	258.66	291.60	281.10	266.19	243.32	3.16
							7,1	206.70	222.93	219.37	215.55	189.71	2.82
2,0	133.27	147.85	144.81	135.15	129.57	2.29	7,2	170.00	180.76	178.66	178.28	154.89	2.54
2,1	100.21	109.11	108.03	101.54	97.72	1.90	7,3	141.47	149.29	148.16	148.39	129.20	2.29
							7,4	118.09	124.45	123.67	123.37	108.91	2.05
3,0	154.67	171.72	167.78	157.42	149.17	2.48	7,5	98.08	103.57	103.11	101.62	91.97	1.81
3,1	120.08	130.09	128.75	122.67	115.18	2.13	7,6	79.78	84.98	84.69	81.55	76.74	1.56
3,2	93.54	101.06	100.36	95.03	90.80	1.80							
							8,0	293.15	331.23	319.24	302.48	274.19	3.33
4,0	177.09	197.19	192.21	180.79	169.62	2.66	8,1	234.31	253.22	248.51	245.42	213.03	2.98
4,1	139.53	150.84	149.05	143.41	132.12	2.32	8,2	193.05	204.87	202.61	203.66	173.72	2.70
4,2	111.96	120.04	119.15	114.94	106.51	2.02	8,3	161.23	169.95	168.48	170.44	145.06	2.45
4,3	88.78	95.42	94.97	90.38	85.91	1.72	8,4	135.49	142.27	141.41	142.92	122.74	2.21
							8,5	113.90	119.54	119.00	119.44	104.50	1.99
5,0	201.42	225.35	218.50	206.20	191.71	2.83	8,6	95.12	100.18	99.79	98.76	88.92	1.77
5,1	159.95	172.56	170.31	165.29	149.80	2.49	8,7	77.74	82.67	82.41	79.55	74.67	1.52
5,2	130.10	138.91	137.62	134.62	121.78	2.20							
5,3	106.14	113.02	112.32	109.37	100.37	1.93	9,0	332.84	377.34	363.08	344.38	309.60	3.50
5,4	85.13	91.25	90.69	86.79	82.17	1.66	9,1	265.72	286.96	281.69	279.52	239.35	3.14
							9,2	218.95	232.59	229.52	232.31	194.68	2.85
6,0	228.36	255.84	247.97	234.41	216.07	3.00	9,3	183.16	192.80	191.14	195.02	162.45	2.60
6,1	182.13	196.72	193.49	189.09	168.81	2.66	9,4	154.46	162.00	160.89	164.36	137.60	2.37
6,2	149.22	158.75	157.26	155.50	137.74	2.37	9,5	130.69	136.82	136.08	138.46	117.57	2.15
6,3	123.32	130.57	129.67	128.27	114.47	2.12	9,6	110.45	115.65	115.15	116.18	100.90	1.94
6,4	101.67	107.78	107.14	105.09	95.71	1.87	9,7	92.64	97.36	97.00	96.36	86.37	1.73
6,5	82.20	87.80	87.40	83.92	79.19	1.61	9,8	76.00	80.70	80.47	77.82	72.91	1.49

Table 1: Characteristic  $\lambda$  wavelengths corresponding to the  $\nu, \nu'$  ( $\nu' < \nu$ ) different vibrational diabatic and adiabatic levels.  $R_n$  denotes the positions of the nodes of  $\psi_\nu$  diabatic wave functions.

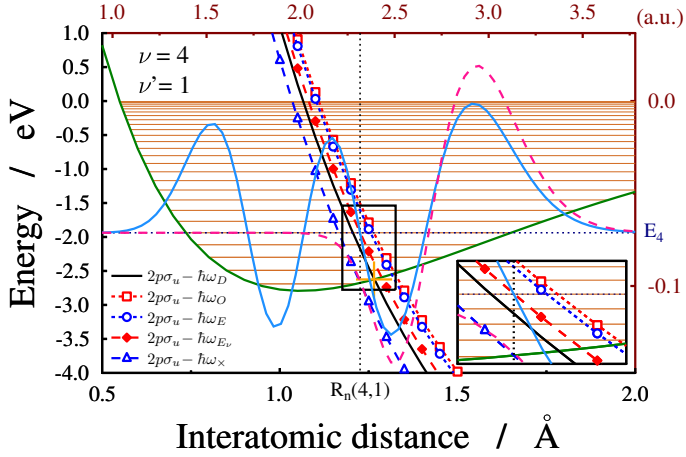


Figure 6: The  $\psi_\nu(\nu = 4)$  diabatic eigenstate (cyan (light gray) line) and  $\varphi_{\nu'}(\nu' = 1)$  adiabatic eigenstate (dashed pink curve) for the case of maximal overlap ( $\lambda_O(4, 1)$ ) with the diabatic  $\nu = 4$  eigenstate. The zero line for the wave functions is placed to the energy level of the  $\nu = 4$  vibrational state. The  $V_1$  diabatic and  $V_2$  potential energies with five field-dressed excited states are also shown. The solid black line denotes the shift by a laser field with the wavelength  $\lambda_D(4, 1)$  ( $\omega_D(4, 1)$  frequency), for which the dissociation of the  $D_2^+$  is minimal. Lines marked with empty squares and circles are shifted by the energies of  $\hbar\omega_O$  and  $\hbar\omega_E$ , respectively. The line marked with solid diamonds corresponds to a shift with  $\hbar\omega_{E_4}$ , so that the energy of the dressed state at the third node ( $R_n(4, 1)$ ) of the  $\nu_4$  diabatic eigenfunction equals to the  $E_4$  vibrational eigen energy. The  $\hbar\omega_\times$  is the photon energy ( $\lambda_\times(4, 1)$  wavelength) by which shifting the  $V_2$  state (marked with triangles) a crossing with the ground state potential is formed at the position of the  $R_n(4, 1)$  node. The inset in the bottom right corner displays a zoomed version of the central area.

# References

- [1] J. L. Krause, K. J. Schafer, and K. C. Kulander: Phys. Rev. Lett. 68, 3535 (1992).
- [2] K. J. Schafer, B. Yang, L. F. DiMauro, and K. C. Kulander: Phys. Rev. Lett. 70, 1599 (1993).
- [3] P. B. Corkum: Phys. Rev. Lett. 71,1994 (1993).
- [4] M. Lewenstein, Ph. Balcou, M. Yu. Ivanov, A. L’Huillier, and P. B. Corkum: Phys. Rev. A. 49, 2117 (1994).
- [5] A. D. Bandrauk, and M. L. Sink: Chem. Phys. Lett., **57**, 569 (1978).
- [6] A. D. Bandrauk, and M. L. Sink: J. Chem. Phys., **74**, 1110 (1981).
- [7] A. D. Bandrauk, E. Constant, and J. M. Gauthier: J. Phys. (France) II **1**, 1033 (1991).
- [8] E. E. Aubanel, J. M. Gauthier, and A. D. Bandrauk: Phys. Rev. A **48**, 2145 (1993).
- [9] E. E. Aubanel, A. Conjusteau, and A. D. Bandrauk: Phys. Rev. A **48**, R4011 (1993).
- [10] A. Giusti-Suzor, and F. H. Mies: Phys. Rev. Lett., **68**, 3869 (1992).
- [11] P. H. Bucksbaum, A. Zavriyev, H. G. Muller, and D. W. Schumacher: Phys. Rev. Lett., **64**, 1883 (1990).
- [12] A. Zavriyev, P. H. Bucksbaum, H. G. Muller, and D. W. Schumacher: Phys. Rev. A **42**, 5500 (1990).
- [13] B. Yang, M Saeed, L. F. DiMauro, A. Zavriyev, and P. H. Bucksbaum, Phys. Rev. A **44**, R1458 (1991).
- [14] A. Zavriyev, P. H. Bucksbaum, Phys. Rev. Lett., **70**, 1077 (1993).
- [15] A. Giusti-Suzor, F. H. Mies, L. F. DiMauro, E. Charron, and B. Yang, J. Phys. B **28**, 309 (1995).
- [16] J. H. Posthumus, Rep. Prog. Phys. **67**, 623 (2004).



- [17] J. H. Posthumus and J. F. McCann, In *Molecules and Clusters in Intense Laser Fields*, ed. J. H. Posthumus, (Cambridge: Cambridge University Press, 2001).
- [18] F. Anis, and B. D. Esry, *Phys. Rev. A* **77**, 033416 (2008).
- [19] R. Numico, A. Keller and O. Atabek, *Phys. Rev. A* **52**, 1298 (1995).
- [20] H. Abou-Rachid, T. T. Nguyen-Dang and O. Atabek, *J. Chem. Phys.* **114**, 2197 (2001).
- [21] C. T. Whelan, *Fragmentation Processes (Topic in Atomic and Molecular Physics)*, (Cambridge: Cambridge University Press, 2013).
- [22] M. F. Kling, C. Siedschlag, A. J. Verhoef, J. I. Khan, M. Schultze, et al., *Science*, **312**, 246 (2006).
- [23] A. Staudte, D. Pavičić, S. Chelkowski, D. Zeidler, M. Meckel, et al., *Phys. Rev. Lett.* **98**, 073003 (2007).
- [24] A. Natan, U. Lev, V. S. Prabhudesai, B. D. Bruner, D. Strasser, D. Schwalm, I. Ben-Itzhak, O. Heber, D. Zajfman, and Y. Silberberg, *Phys. Rev. A* **86**, 043418 (2012).
- [25] S. I. Chu, *J. Chem. Phys.* **75**, 2215 (1981).
- [26] S. I. Chu, and D. A. Telnov, *Phys. Rep.* **390**, 1 (2004).
- [27] A. D. Bandrauk, E. Aubanel, and J. M. Gauthier, *Molecules in Laser Fields* (Marcel Dekker Inc., New York, 1994).
- [28] L. J. Frasinski, J. H. Posthumus, J. Plumridge, K. Codling, P. F. Taday, and A. J. Langley, *Phys. Rev. Lett.*, **83**, 3625 (1999).
- [29] K. Sandig, H. Figger, and T. W. Hansch, *Phys. Rev. Lett.*, **85**, 4876 (2000).
- [30] N. Moiseyev, M. Sindelka and L. S. Cederbaum, *J. Phys. B* **41**, 221001 (2008).
- [31] M. Sindelka, N. Moiseyev and L. S. Cederbaum, *J. Phys. B* **44**, 045603 (2011).

- [32] G. J. Halász, Á. Vibók, M. Sindelka, N. Moiseyev and L. S. Cederbaum, J. Phys. B **44**, 175102 (2011).
- [33] G. J. Halász, M. Sindelka, N. Moiseyev, L. S. Cederbaum and Á. Vibók, J. Phys. Chem. A **116**, 2636 (2012).
- [34] G. J. Halász, Á. Vibók, M. Sindelka, L. S. Cederbaum and N. Moiseyev, Chem. Phys. **399**, 146 (2012).
- [35] G. J. Halász, Á. Vibók, N. Moiseyev and L. S. Cederbaum, J. Phys. B **45**, 135101 (2012).
- [36] G. J. Halász, Á. Vibók, N. Moiseyev and L. S. Cederbaum, Phys. Rev. A **88**, 043413 (2013).
- [37] G. J. Halász, Á. Vibók, H.-D. Meyer, and L. S. Cederbaum: J. Phys. Chem. A **117**, 8528 (2013).
- [38] G. J. Halász, A. Csehi, Á. Vibók, and L. S. Cederbaum: J. Phys. Chem. A **118**, 11908 (2014).
- [39] G. J. Halász, Á. Vibók, and L. S. Cederbaum: J. Phys. Chem. Lett., **6**, 348 (2015).
- [40] G. J. Halász, A. Csehi, and Á. Vibók: Theor. Chem. Acc. **134**, 128 (2015).
- [41] A. Csehi, G. J. Halász, L. S. Cederbaum and Á. Vibók, J. Chem. Phys. **143**, 014305 (2015).
- [42] M. Pawlak and N. Moiseyev, Phys. Rev. A **92**, 023403 (2015).
- [43] J. Kim, H. Tao, J. L. White, V. S. Petrovi, T. J. Martinez and P. H. Bucksbaum, J. Phys. Chem. A **116**, 2758 (2012).
- [44] A. Natan, M. R. Ware and P. H. Bucksbaum, Ultrafast Phenomena XIX, Springer Proceedings in Physics **162**, 122 (2015).
- [45] J. Kim, H. Tao, T. J. Martinez and P. H. Bucksbaum, J. Phys. B **48**, 164003 (2015).
- [46] M. E. Corrales, J. González-Vázquez, G. Balerdi, I. R. Solá, R. de Nalda and L. Bañares, Nat. Chem. **6**, 785 (2014).
- [47] I. R. Solá, J. González-Vázquez, R. de Nalda and L. Bañares, Phys. Chem. Chem. Phys. **17**, 13183 (2015).

- [48] P. V. Demekhin and L. S. Cederbaum, J. Chem. Phys. **139**, 154314 (2013).
- [49] S. I. Chu, C. Laughlin and Datta, K. Chem. Phys. Lett. **98**, 476 (1983).
- [50] F. V. Bunkin and I. I. Tugov, Phys. Rev. A **8**, 601 (1973).
- [51] H. D. Meyer, U. Manthe and L. S. Cederbaum, Chem. Phys. Lett. **165**, 73 (1990).
- [52] U. Manthe, H. D. Meyer and L. S. Cederbaum, J. Chem. Phys. **97**, 3199 (1992).
- [53] M. H. Beck, A. Jäckle, G. A. Worth and H. D. Meyer, Phys. Rep. **324**, 1 (2000).
- [54] G. A. Worth, *et. al.* The MCTDH package, version 8.2, (**2000**), Meyer, H. D.; *et. al.* version 8.3, (**2002**), version 8.4 (**2007**), University of Heidelberg, Germany; <http://mctdh.uni-hd.de/>.
- [55] H. D. Meyer, F. Gatti, and G. A. Worth, Multidimensional Quantum Dynamics: MCTDH Theory and Applications (Weinheim: Wiley-VCH), (**2009**).